Measurement of lifetimes in ^{62,64}Fe , ^{61,63}Co, and ^{59}Mn

M. Klintefjord,[1,*] J. Ljungvall,[2] A. Görgen,[1] S. M. Lenzi,[3] F. L. Bello Garrote,[1] A. Blazhev,[4] E. Clément,[5] G. de France,[5] J.-P. Delaroche,[6] P. Désesquelles,[2] A. Dewald,[4] D. T. Doherty,[7] C. Fransen,[4] A. Gengelbach,[8] G. Georgiev,[2] M. Girod,[6] A. Goasduff,[9] A. Gottardo,[10] K. Hadyńska-Klęk,[1] B. Jacquot,[5] T. Konstantinopoulos,[2] A. Korichi,[2] A. Lemasson,[5] J. Libert,[10] A. Lopez-Martens,[2] C. Michelagnoli,[5] A. Navin,[5] J. Nyberg,[8] R. M. Pérez-Vidal,[11] S. Roccia,[2] E. Sahin,[1] I. Stefan,[10] A. E. Stuchbery,[12] M. Zielińska,[7] D. Barrientos,[13] B. Birkenbach,[4] A. Boston,[14] L. Charles,[15] M. Ciemala,[16] J. Dudouet,[17] J. Eberth,[4] A. Gadea,[11] V. González,[18] L. Harkness-Brennan,[14] H. Hess,[4] A. Jungclaus,[19] W. Korten,[7] R. Menegazzo,[20] D. Mengoni,[20,3] B. Million,[20] A. Pullia,[21,22] D. Ralet,[2,23,24] F. Recchia,[20,3] P. Reiter,[4] M. D. Salsac,[7] E. Sanchis,[18] O. Stezowski,[17] Ch. Theisen,[7] and J. J. Valiente Dobon[9]

[1]*Department of Physics, University of Oslo, N-0316 Oslo, Norway*
[2]*CSNSM, Univ. Paris-Sud, CNRS/IN2P3, Université Paris-Saclay, 91405 Orsay, France*
[3]*Dipartimento di Fisica e Astronomia dell'Università and INFN, Sezione di Padova, I-35131 Padova, Italy*
[4]*Institut für Kernphysik, Universität zu Köln, D-50937 Köln, Germany*
[5]*GANIL, CEA/DRF-CNRS/IN2P3, Bd. Henri Becquerel, BP 55027, F-14076 Caen, France*
[6]*CEA, DAM, DIF, F-91297 Arpajon, France*
[7]*Irfu, CEA, Université Paris-Saclay, F-91191 Gif-sur-Yvette, France*
[8]*Institutionen för fysik och astronomi, Uppsala Universitet, SE-751 05 Uppsala, Sweden*
[9]*INFN Laboratori Nazionali di Legnaro, Viale dell'Università, 2, I-35020 Legnaro, Italy*
[10]*Institut de Physique Nucléaire, CNRS/IN2P3-Université Paris-Sud, F-91406 Orsay, France*
[11]*Instituto de Física Corpuscular, CSIC-Universidad de Valencia, E-46071 Valencia, Spain*
[12]*Department of Nuclear Physics, Australian National University, Canberra ACT 0200, Australia*
[13]*CERN, CH-1211 Geneva 23, Switzerland*
[14]*Oliver Lodge Laboratory, The University of Liverpool, Liverpool, L69 7ZE, United Kingdom*
[15]*IPHC, UNISTRA, CNRS, 23 rue du Loess, 67200 Strasbourg, France*
[16]*The Henryk Niewodniczański Institute of Nuclear Physics, Polish Academy of Sciences, ul. Radzikowskiego 152, 31-342 Kraków, Poland*
[17]*Université de Lyon, Université Lyon-1, CNRS/IN2P3, UMR5822, IPNL, 4 Rue Enrico Fermi, F-69622 Villeurbanne Cedex, France*
[18]*Departamento de Ingeniería Electrónica, Universitat de Valencia, Burjassot, Valencia, Spain*
[19]*Instituto de Estructura de la Materia, CSIC, Madrid, E-28006 Madrid, Spain*
[20]*INFN Sezione di Padova, I-35131 Padova, Italy*
[21]*University of Milano, Dept. of Physics, I-20133 Milano, Italy*
[22]*INFN Milano, I-20133 Milano, Italy*
[23]*Institut für Kernphysik, Technische Universität Darmstadt, Darmstadt D-64289, Germany*
[24]*GSI Helmholtzzentrum für Schwerionenforschung GmbH, Planckstraße 1, D-64291 Darmstadt, Germany*

(Received 16 November 2016; revised manuscript received 3 January 2017; published 9 February 2017)

Lifetimes of the 4_1^+ states in ^{62,64}Fe and the $11/2_1^-$ states in ^{61,63}Co and ^{59}Mn were measured at the Grand Accélérateur National d'Ions Lourds (GANIL) facility by using the Advanced Gamma Tracking Array (AGATA) and the large-acceptance variable mode spectrometer (VAMOS++). The states were populated through multinucleon transfer reactions with a ^{238}U beam impinging on a ^{64}Ni target, and lifetimes in the picosecond range were measured by using the recoil distance Doppler shift method. The data show an increase of collectivity in the iron isotopes approaching $N = 40$. The reduction of the subshell gap between the $\nu 2p_{1/2}$ and $\nu 1g_{9/2}$ orbitals leads to an increased population of the quasi-SU(3) pair $(\nu 1g_{9/2}, \nu 2d_{5/2})$, which causes an increase in quadrupole collectivity. This is not observed for the cobalt isotopes with $N < 40$ for which the neutron subshell gap is larger due to the repulsive monopole component of the tensor nucleon-nucleon interaction. The extracted experimental $B(E2)$ values are compared with large-scale shell-model calculations and with beyond-mean-field calculations with the Gogny D1S interaction. A good agreement between calculations and experimental values is found, and the results demonstrate in particular the spectroscopic quality of the Lenzi, Nowacki, Poves, and Sieja (LNPS) shell-model interaction.

DOI: 10.1103/PhysRevC.95.024312

*malin.klintefjord@fys.uio.no

I. INTRODUCTION

A cornerstone of nuclear structure physics is the existence of "magic" nuclei with increased binding due to large gaps in the single-particle shell structure. Spectroscopy of exotic nuclei away from the line of β stability has shown that the magic numbers are not universal throughout the nuclear chart but depend on the ratio of neutron to proton numbers; that is, they may vary as a function of isospin [1]. Far from stability, the relative strength of the different terms in the nuclear force may vary and cause a modification of the shell structure. The theoretical description of the changing shell structure is challenging and requires appropriate valence spaces and effective interactions for shell-model calculations and improved energy functionals for mean-field-based models.

Regions in the nuclear chart with rapid changes in collectivity as a function of Z or N are of particular interest because they allow stringent testing of theoretical models. The neutron-rich nuclei close to ^{68}Ni show a rapid variation in collectivity, which is understood in the shell model as the combination of the effect of the monopole part of the central and tensor force [2,3], leading to a reduced shell gap at $N = 40$ as protons are removed, and quadrupole correlations arising from the multipole part. This favors a substantial gain in correlation energy via the excitation of neutrons across the $N = 40$ gap to the quasi-SU(3) partner orbitals $\nu g_{9/2}$ and $\nu d_{5/2}$. It should also be noted that, for protons, this is accompanied by an increase in excitations across the $Z = 28$ gap to the $p_{3/2}$ orbital, which is the quasi-SU(3) partner of the $f_{7/2}$ orbital. This mechanism has been theoretically investigated and compared with available experimental data for cobalt, iron, manganese, and chromium isotopes. It was concluded that the arising collective structures can only be reproduced by including the $\nu d_{5/2}$ together with the $\nu g_{9/2}$ orbital in the model space as one approaches $N = 40$ [4–7]. It was shown that the wave functions of the low-lying states contain a large contribution from these intruder states, while the configurations that correspond to "normal" shell filling lie higher in energy. This is the same mechanism that causes the disappearance of the $N = 8$ and $N = 20$ shell closures for neutron-rich nuclei, giving rise to so-called islands of inversion not only at the $N = 8$ and $N = 20$, but also at the $N = 40$ harmonic-oscillator shell closure [8].

A substantial amount of experimental data exist for the region, starting with $^{68}_{28}$Ni$_{40}$ with a high excitation energy of the 2^+_1 state and a small $B(E2; 2^+_1 \rightarrow 0^+_1)$ value, suggesting a closed-shell nucleus [9,10]. On the other hand, no strong $N = 40$ shell gap is seen in mass measurements [11,12], and the weak $B(E2; 2^+_1 \rightarrow 0^+_1)$ value in ^{68}Ni is understood as being due to a strong neutron component in the 2^+_1 excitation [13]. Spectroscopic studies of neutron-rich cobalt isotopes have shown that the $N = 40$ subshell gap inhibits the development of low-lying collective structures up to $^{65}_{27}$Co$_{38}$. Here, increasing neutron occupation of orbitals above the $N = 40$ gap manifests itself through the coexistence of spherical and deformed structures at low excitation energy. Even in ^{67}Co the yrast states can be reasonably well described as a proton particle (hole) weakly coupled to the 2^+_1 state in the corresponding iron (nickel) isotones [14–18].

Spectroscopy experiments following β decay [19–21], multinucleon transfer [22,23], and knock-out reactions [24] have found a sudden drop in the excitation energy of the 2^+_1 states in neutron-rich iron isotopes from $N = 38$. This is consistent with lifetime measurements [8,25] and intermediate-energy Coulomb excitation experiments [26] that show a strong increase of the $B(E2)$ values. Recent measurements performed at RIKEN have extended the systematics of excitation energies in chromium and iron isotopes towards the $N = 50$ shell gap [27], indicating a continuation of the $N = 40$ island of inversion toward $N = 50$. Extensive spectroscopic studies of manganese isotopes up to ^{63}Mn indicate an increase in collectivity already at lower neutron numbers [28,29]. Recent collinear laser spectroscopy of odd-even manganese isotopes up to ^{65}Mn and the measurement of the g factor of the ground state indicate that there is an increasing fraction of neutron excitation across the $N = 40$ subshell gap for manganese isotopes with $N \geqslant 36$ [30].

The enhanced collectivity of even-even nuclei around ^{66}Fe and ^{64}Cr was also the subject of theoretical investigations using mean-field-based approaches [31–34]. Hartree–Fock–Bogoliubov (HFB) calculations with the Gogny D1S interaction found the $N = 40$ subshell gap to be almost constant in size between $Z = 20$ and $Z = 40$ [35]. The potential-energy surfaces for ^{64}Cr and ^{66}Fe were found with a spherical minimum that is soft toward prolate deformation. Applying the generator coordinate method with a five-dimensional collective Hamiltonian (5DCH) yielded $B(E2; 2^+_1 \rightarrow 0^+_1)$ values for ^{64}Cr and ^{66}Fe that are in relatively good agreement with the experimental values, whereas the excitation energies were significantly overestimated [35].

While a coherent picture of nuclear structure around ^{68}Ni starts to emerge, there are still only few electromagnetic transition probabilities known in the region. Experimental $B(E2)$ values for the neutron-rich iron isotopes are only known for the $2^+_1 \rightarrow 0^+_1$ transitions [8,25,26], but not for higher-lying transitions. For the cobalt isotopes, lifetimes were reported for the $9/2^-$ and $11/2^-$ states in ^{61}Co [36], the $3/2^-$ and $9/2^-$ states in ^{63}Co [16], the $11/2^-$ state in ^{63}Co [18], and the $11/2^-$ and $13/2^-$ states in ^{65}Co [18]. For the manganese isotopes some transition strengths are known from Coulomb excitation of ^{61}Mn [37], and lifetimes were very recently reported for the $7/2^-$, $9/2^-$, and $11/2^-$ states in ^{63}Mn [38]. No transition strengths have been reported for ^{59}Mn so far. As theoretical descriptions of this region, in particular recent shell-model calculations [27], are showing an impressive agreement for excitation energies over a large range of isotopes, it is of great interest to challenge these models with experimental transition strengths, which are more sensitive to details of the wave functions than excitation energies alone. The measurements of additional experimental electromagnetic transition probabilities therefore provide important benchmarks for both shell-model and beyond-mean-field calculations.

The recoil-distance Doppler shift (RDDS) technique has been successfully applied in recent years in combination with multinucleon transfer reactions and the identification of reaction products in magnetic spectrometers [39]. Here, we report on the first RDDS lifetime measurement with AGATA

coupled to VAMOS++ at GANIL. New lifetimes were measured in ^{62,64}Fe, ^{61,63}Co, and ^{59}Mn by using multinucleon transfer reaction between ^{238}U projectiles and ^{64}Ni target nuclei. The article is organized as follows: Experimental details and the data analysis are described in Secs. II and III, respectively. The results are presented in Sec. IV and discussed and compared with theoretical calculations in Sec. V.

II. EXPERIMENTAL DETAILS

Excited states of nuclei in the $A \approx 60$ region were populated in multinucleon transfer-reactions from a 6.5A MeV ^{238}U beam with an intensity of 0.2–0.5 pnA impinging on a 1.25-mg/cm^2-thick ^{64}Ni target at GANIL. The VAMOS++ spectrometer [40–42] was used to detect and identify the target-like transfer products. It was positioned at 45° with respect to the beam axis, close to the grazing angle of the reaction. During this experiment the detection system of VAMOS++ consisted of a set of dual position-sensitive multiwire proportional counter detectors at the entrance of the spectrometer used for the time-of-flight measurement and giving the direction of the ions for Doppler correction, two sets of drift chambers used to determine the trajectory of the ions after the dipole magnet followed by multiwire proportional chambers to give the time of flight, and finally ionization chambers for measuring the total energy and energy loss of the ions at the focal plane. This focal plane detection in VAMOS++ allows for the reconstruction of the particle trajectories and the magnetic rigidity. In this experiment two settings of the magnetic rigidity were used with $B\rho = 0.97$ T m and $B\rho = 0.92$ T m.

Gamma rays were detected in the AGATA germanium γ-ray tracking array [43], which at the time of the experiment consisted of 19 crystals placed 23.5 cm from the target position. The detectors covered the backward angles from 145° to 180° with respect to the spectrometer axis. Count rates in each crystal were about 6–10 kHz depending on current beam intensity, and trapezoidal shaping with a rise time of 2.5 μs and a peak time of 3 μs was used. A γ-particle coincidence rate between AGATA and VAMOS++ of a few hundred hertz allowed for pulse-shape analysis of the signals from the segmented AGATA detectors to be performed online. The γ-ray tracking procedure was performed after each run (typically 12 hours of data taking) during the experiment reading data from disk. The high position resolution of AGATA, together with the reconstruction of the velocity vector for the ions in VAMOS++, resulted in a γ-ray resolution of 5.6 keV for the Doppler corrected 1345 keV γ-ray line in ^{64}Ni. The data, including the digitized germanium detector signals, were written to disk for further improved analysis [44].

The Orsay universal plunger system (OUPS) [45] was used for the lifetime measurements using the RDDS method. Particles recoiling out of the target were slowed down by a 3.0-mg/cm^2-thick ^{24}Mg degrader before entering the VAMOS++ spectrometer with a mean recoil velocity after the degrader of 10.7% of the speed of light. Target and degrader foils were mounted orthogonal to the entry axis of VAMOS++. Data were taken with six different target-degrader distances, $d_0 + 10.1(4)$ μm, $d_0 + 19.9(2)$ μm, $d_0 + 40.0(2)$ μm, $d_0 + 59.9(3)$ μm, $d_0 + 80.3(5)$ μm, and $d_0 + 206(4)$ μm, for about 24 h per distance. The offset d_0 was determined by using known lifetimes; see Sec. III. For the five shortest distances an active feedback system was used to control the distance.

III. DATA ANALYSIS

The target-like reaction products were identified in mass, charge, and atomic number with the VAMOS++ spectrometer. Nuclei with the same atomic number Z were identified by their characteristic energy loss from the ΔE-E energy spectrum, shown in Fig. 1. The mass-over-charge ratio of the ions was determined from the time of flight, the path through the spectrometer, and the magnetic rigidity. Combined with the total energy of the ions the mass can be determined, and the mass distributions for the manganese, iron, and cobalt chains are shown in Fig. 2. Gamma rays detected with AGATA in coincidence with ^{62,64}Fe, ^{61,63}Co, and ^{59}Mn, summed over all six distances, are shown in Fig. 3.

Gamma rays from the decaying excited states in the recoiling nuclei are emitted in flight. Due to the energy loss in the degrader, Doppler shifts are different for decays before and after the degrader, respectively. The spectra were incremented with γ rays that were Doppler corrected event by event by using the velocity vector of the recoiling ions after the degrader measured with the VAMOS++ spectrometer. Gamma rays emitted before the degrader have a higher velocity than those used in the Doppler correction and appear at lower energies when observed under backward angles. In the cases where the lifetime is comparable to the time of flight between the target and degrader, this procedure results in two distinct peaks for each decay, with decays occurring before the degrader contributing to the *shifted* peak (at lower energy) and decays occurring after the degrader contributing to the *unshifted* peak.

The effect of γ rays emitted during deceleration of the ions in the degrader foil was investigated for the different distances by using the AGATA Monte Carlo simulations package [46] and found negligible compared with the statistical and other

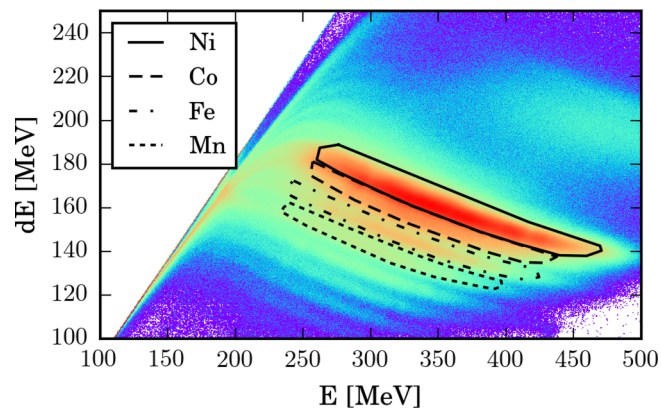

FIG. 1. Energy loss of the target-like reaction products in VAMOS++ as a function of total energy detected, with cuts on manganese (dotted), iron (dash-dotted), cobalt (dashed), and nickel (solid) isotopes.

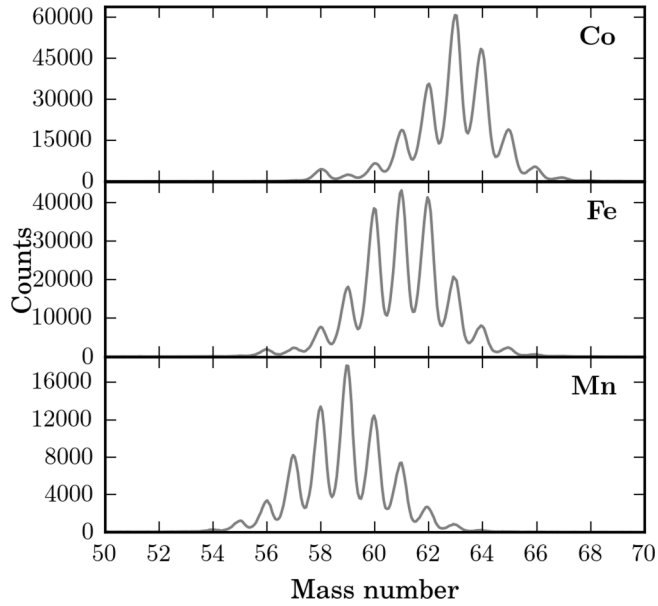

FIG. 2. Mass distributions for the manganese, iron, and cobalt isotopic chains.

systematic errors, except for the 2^+ state in ^{64}Ni, where systematic uncertainties from this effect dominates the statistical ones, and are of the order of 10%.

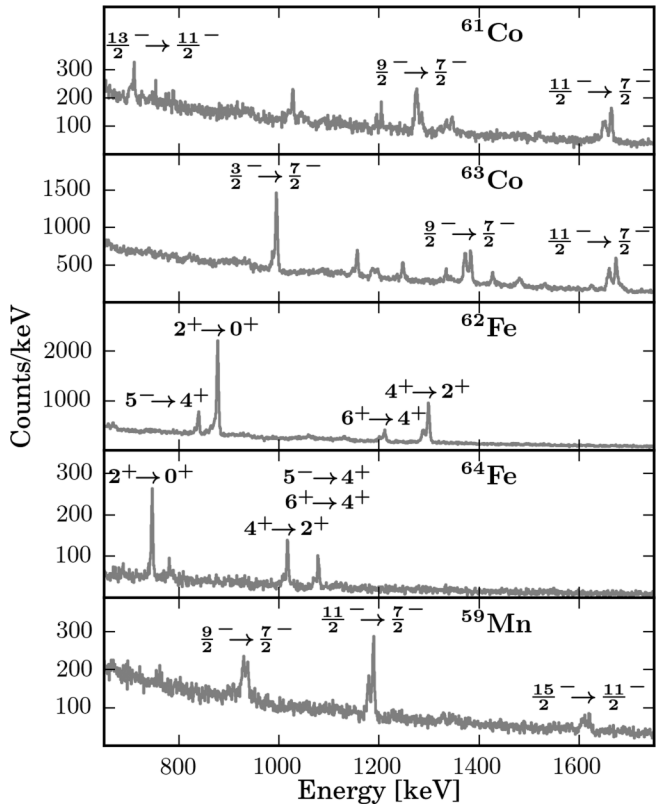

FIG. 3. γ-ray spectra in coincidence with ions identified as ^{59}Mn, ^{62,64}Fe, and ^{61,63}Co, summed over all six distances.

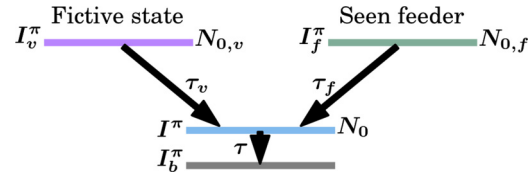

FIG. 4. Schematic level scheme illustrating the feeding and decay of the level of interest. Unobserved feeding is accounted for by introducing a fictive level (marked with v).

Decay curves $R(x)$ for the level of interest and for observed feeding transitions, $R_f(x)$, were constructed according to

$$R^{(\mathrm{expt})}(x) = \frac{I_u^{(\mathrm{expt})}(x)}{I_s^{(\mathrm{expt})}(x) + I_u^{(\mathrm{expt})}(x)},$$
$$R_f^{(\mathrm{expt})}(x) = \frac{1}{\epsilon_{\mathrm{rel.}}^{(\mathrm{expt})}} \frac{I_{u,\mathrm{f}}^{(\mathrm{expt})}(x)}{I_s^{(\mathrm{expt})}(x) + I_u^{(\mathrm{expt})}(x)}, \quad (1)$$

where $I_s^{(\mathrm{expt})}(x)$ and $I_u^{(\mathrm{expt})}(x)$ are the measured shifted and unshifted intensities, respectively, of the decay transition from the level of interest, $I_{u,\mathrm{f}}^{(\mathrm{expt})}(x)$ is the intensity of the unshifted component of the observed feeder, and $\epsilon_{\mathrm{rel.}}^{(\mathrm{expt})}$ is the relative detection efficiency for the feeding transition relative to the decay transition.

Lifetimes were fit to the observed γ decays by solving the coupled linear differential equations arising from the decay of the level of interest and its feeders, as illustrated in Fig. 4. The model for the level schemes used in this work consists of the level of interest, any observed transitions from feeder states, and *unseen feeding*, which is treated by introducing a fictive level approximating possible delayed feeding to the level of interest from other levels. More complicated feeding schemes have been tried, giving compatible results but with a higher χ^2/N_{dof} by a factor two or more. Therefore, the simplest scheme has been used. Given the proportion of decays coming from the feeders, $N_{0,\mathrm{f}}$ and $N_{0,\mathrm{v}}$, and the lifetimes, τ, τ_f, and τ_{v}, the fitted decay curves are

$$R(t) = e^{-t/\tau} + N_{0,\mathrm{f}}\tau_f \frac{e^{-t/\tau_f} - e^{-t/\tau}}{\tau_f - \tau} + N_{0,\mathrm{v}}\tau_{\mathrm{v}} \frac{e^{-t/\tau_{\mathrm{v}}} - e^{-t/\tau}}{\tau_{\mathrm{v}} - \tau},$$
$$F(t) \equiv 1 - R(t), \quad (2)$$
$$R_f(t) = N_{0,\mathrm{f}} e^{-t/\tau_f},$$

where F is called the flight curve. Note that $N_{0,\mathrm{v}}$ only includes the delayed unseen feeding. Any prompt unseen feeding, given by $1 - N_{0,\mathrm{f}} - N_{0,\mathrm{v}}$, does not influence the lifetime measurement.

Experimental data were obtained for $N_{\mathrm{dist}} = 6$ different distances $d_n^{(\mathrm{expt})}$ between target and degrader. The corresponding time of flight to the degrader is

$$t_n^{(\mathrm{expt})} = \frac{d_n^{(\mathrm{expt})} - d_{\mathrm{off.}}^{(\mathrm{expt})}}{v^{(\mathrm{expt})}}, \quad (3)$$

where $v^{(\mathrm{expt})}$ is the velocity of the particles before the degrader. The velocity $v^{(\mathrm{expt})}$ was obtained from the VAMOS++

spectrometer and corrected for the energy loss in the degrader by using the Doppler shift of the γ transition under study. The offset $d_{\text{off.}}^{(\text{expt})}$ was not measured during the experiment. Therefore, a value for the offset was obtained from the well-constrained fit of the lifetime of the 2_1^+ state in ^{64}Ni [47], resulting in $d_{\text{off.}}^{(64\text{Ni})} = -16.5 \pm 0.7\ \mu m$.

The intensities need to be normalized to allow for a direct comparison with experimental intensities. This is done by fitting normalization constants $I_{s+u,n}$, one for each distance of the degrader. By using both the shifted and unshifted components from the level of interest, the normalization constants $I_{s+u,n}$ are constrained by the total number of detected γ decays from this level; namely, $I_{s,n}^{(\text{expt})} + I_{u,n}^{(\text{expt})}$.

The lifetimes that best describe the data are found by using a nonlinear least-square minimization,

$$\begin{aligned}\chi^2(\tau,\tau_f,\tau_v,N_{0,\text{f}},N_{0,\text{v}},\vec{I}_{s+u},v,\epsilon_{\text{rel.}},d_{\text{off.}},\vec{d}\,) &= \sum_{n=1}^{N_{\text{dist}}}\left[\left(\frac{I_{u,n}^{(\text{expt})}-I_{s+u,n}R(t_n)}{\sigma_{I_{u,n}^{(\text{expt})}}}\right)^2+\left(\frac{I_{s,n}^{(\text{expt})}-I_{s+u,n}F(t_n)}{\sigma_{I_{s,n}^{(\text{expt})}}}\right)^2\right.\\ &\left.+\left(\frac{I_{u,n,\text{f}}^{(\text{expt})}-\epsilon_{\text{rel.}}I_{s+u,n}R_f(t_n)}{\sigma_{I_{u,n,\text{f}}^{(\text{expt})}}}\right)^2\right]\\ &+\left(\frac{v^{(\text{expt})}-v}{\sigma_{v^{(\text{expt})}}}\right)^2+\left(\frac{\epsilon_{\text{rel.}}^{(\text{expt})}-\epsilon_{\text{rel.}}}{\sigma_{\epsilon_{\text{rel.}}^{(\text{expt})}}}\right)^2+\left(\frac{d_{\text{off.}}^{(64\text{Ni})}-d_{\text{off.}}}{\sigma_{d_{\text{off.}}^{(64\text{Ni})}}}\right)^2\\ &+\sum_{n=1}^{N_{\text{dist}}}\left(\frac{d_n^{(\text{expt})}-d_n}{\sigma_{d_n^{(\text{expt})}}}\right)^2, \qquad (4)\end{aligned}$$

where $t_n = (d_n - d_{\text{off.}})/v$. By fitting the velocity, distances, distance offset, γ efficiency and normalization coefficients, the systematical uncertainties from these quantities were taken into account in the fitting procedure. Thus, the uncertainties in the obtained lifetimes incorporate all of these sources of experimental uncertainties. This also makes it possible to determine how much the different sources of experimental uncertainties influence the values and uncertainties of the obtained lifetimes, which we demonstrate in the following section. Here statistical errors refer to the errors extracted from the fit using Eq. (4) excluding the four last terms whereas the statistical errors are extracted from the increase in error on the lifetime using the full expression.

IV. RESULTS

The analysis procedure was tested by applying it to the lifetime of the first 2^+ state in ^{64}Ni. The resulting lifetime of $1.537(76)_{\text{stat}}(150)_{\text{sys}}$ ps agrees well with 1.570(50) ps obtained in Ref. [48] and the adopted value of 1.469(75) ps from Ref. [47]. However, it is in disagreement with the value of 1.287(52) ps from a recent Coulomb excitation experiment by Allmond *et al.* [49].

Because the lifetime of the 2^+ state in ^{64}Ni was used to constrain the offset parameter d_{off} for the distance, it was investigated how much the choice of its value influences the results for other nuclides. Using the newer value of Allmond *et al.* to determine the offset parameter yields shorter lifetimes for the other nuclides, but differences are within the error bars and would not change any conclusions; e.g., for ^{62}Fe the lifetime of the 4_1^+ states goes from 0.86(25) to 0.58(16) ps. For other nuclei the changes are similar. Constraining the distance parameter with the longer lifetime value of $1.537(76)_{\text{stat}}(150)_{\text{sys}}$ ps results in a lower χ^2 ($\chi^2/N_{\text{dof}} = 9$ vs $\chi^2/N_{\text{dof}} = 37$) of the fit and was therefore chosen. Approximately 8% of the uncertainty for the 2^+ state in ^{64}Ni originates from the measured intensities of the shifted and unshifted transitions, 68% from the statistical uncertainty in the velocity, and 19% from the distance offset. Applying the analysis method to the 4_1^+ state in ^{60}Fe results in a lifetime of 1.20(30) ps, with $\chi^2/N_{\text{dof}} = 1.29$ and 21% population from the seen $6_1^+ \to 4_1^+$ and $5_1^- \to 4_1^+$ transitions, with an effective lifetime of 15(15) ps. In the fit, 24% of the decay occurred via the long-lived (>9 ps) unseen feeder. In this case the statistical uncertainty is 98% of the total error. The obtained lifetime is in agreement with the result in Ref. [50].

For ^{62}Fe, the shifted and unshifted components of the $4_1^+ \to 2_1^+$ transition at 1299 keV are shown in Fig. 5. For this nucleus, the statistics allowed the inclusion of the $6_1^+ \to 4_1^+$ transition and the $5_1^- \to 4_1^+$ transition as seen feeding transitions, while unobserved feeding was taken into account by introducing a fictive feeding state. The corresponding decay curves are presented in Fig. 6. The fit yields a lifetime of $\tau_{4_1^+} = 0.86(25)$ ps with $\chi^2/N_{\text{dof}} = 1.72$, where $N_{\text{dof}} = 11$. In the fit, 27% of the intensity of the 4_1^+ state comes via the $6_1^+ \to 4_1^+$ transition with an effective lifetime of 9.5(24) ps, 25% via the $5_1^- \to 4_1^+$ transition with an effective lifetime of 58(50) ps, and 14% is attributed to unseen transitions with an effective lifetime of 75(75) ps. In this fit 97% of the error is statistical.

In ^{64}Fe, the lifetime of the 4_1^+ state was obtained from the shift of the $4_1^+ \to 2_1^+$ γ-ray transition at 1017 keV, shown in Fig. 5. The unresolved transitions at 1079 keV (from $6_1^+ \to 4_1^+$) and at 1078 keV (from $5_1^- \to 4_1^+$) were included as seen feeding in the fit, and the decay curves are shown in Fig. 6. As the 5_1^- state is more strongly populated than the 6_1^+ state and has a substantial lifetime it will be the main contributor to long-lived feeding. Subtracting the observed feeding, in combination with poor statistics, results in large uncertainties and hence very weak constraints on the fitting parameters. With unobserved feeding included in the fitting procedure, a short lifetime of 0.19(98) ps was obtained for the 4_1^+ state with $\chi^2/N_{\text{dof}} = 0.63$. The low χ^2 suggest a under-constrained fit, and such a short value lies outside the sensitivity range of the experiment. Assuming no unobserved feeding will always lead to a longer lifetime for the state of interest, providing only an upper limit for the lifetime. In case of the 4^+ state in ^{64}Fe an upper limit of $\tau < 1.8$ ps was found and adopted. In this case the fit yields $\chi^2/N_{\text{dof}} = 1.15$ with $N_{\text{dof}} = 9$, and 57% of the feeding was observed with an effective lifetime of 32(29) ps.

The γ-ray spectra gated on ^{63}Co, shown in Fig. 5, were used to extract the lifetime from the $11/2_1^- \to 7/2_1^-$ transition at 1674 keV γ-ray energy. Figure 6 shows the best fit of the decay curve with an unseen feeder of the order of 7 ps, resulting in $\tau_{11/2_1^-} = 0.55(19)$ ps with $\chi^2/N_{\text{dof}} = 1.6$ and $N_{\text{dof}} = 3$. Here, the relative strength of the unobserved feeding is 62%. This result is consistent, within the joint error bars, with the result found in Ref. [18]. In ^{61}Co, the $11/2_1^- \to (9/2)_1^-$ transition

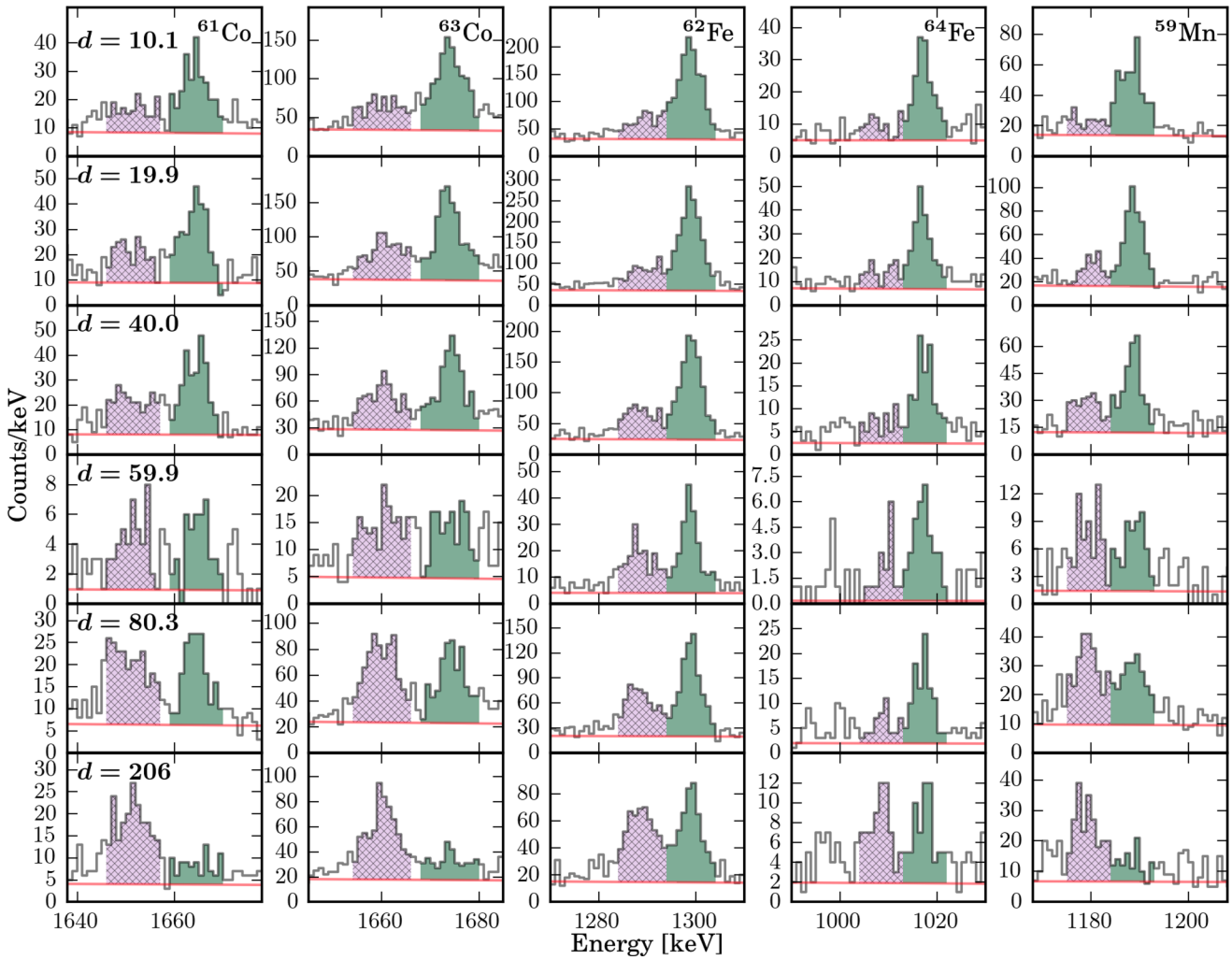

FIG. 5. The spectra used to extract the lifetime of the $11/2_1^-$ state in ^{59}Mn and ^{61,63}Co and the 4_1^+ in ^{62,64}Fe for the different distances d (in μm). Shown as color coded areas are the intensities used for determining the decay curves. The area to the left is the shifted component while the right area is the unshifted component.

at 1664 keV (see Fig. 5) was used to investigate the lifetime of the $11/2_1^-$ state. Seen feeding from the $(13/2)_1^- \rightarrow 11/2_1^-$ transition was included in the fit. Similar to the case of ^{64}Fe, the statistics were not sufficient to extract a precise value of the lifetime, and only an upper limit of $\tau < 2$ ps is found assuming no unobserved feeding. The $\chi^2/N_{\rm dof}$ for this fit is 2.3 with nine degrees of freedom.

Finally, the lifetime from the $11/2_1^- \rightarrow 7/2_1^-$ transition [28] at 1189 keV γ-ray energy in ^{59}Mn was extracted from the spectra shown in Fig. 5. Fitting the lifetime with an assumed long-lived unobserved feeder ($\tau_v > 7$ ps), where 17% of the decay proceeds via this feeder, resulted in a lifetime of $\tau_{11/2_1^-} = 2.63(40)$ ps with $\chi^2/N_{\rm dof} = 0.39$ and $N_{\rm dof} = 3$. The fit to the decay curve is shown in Fig. 6.

V. DISCUSSION

In Fig. 7 experimental and theoretical values for the reduced transition strengths in the iron isotopes $^{56-68}$Fe are shown for the $2_1^+ \rightarrow 0_1^+$ and $4_1^+ \rightarrow 2_1^+$ transitions. The new data points from this work are shown with stars. A small increase in the $B(E2)$ value for the $4_1^+ \rightarrow 2_1^+$ transition from $N = 34$ to $N = 36$ is observed. The upper limit for the lifetime of the 4_1^+ state in ^{64}Fe indicates a larger increase in the $B(E2)$ value from $N = 36$ to $N = 38$. Experimentally, the iron isotopes with $R_{42} = E(4^+)/E(2^+)$ ratios between the harmonic vibrator limit of 2 and the rotational limit of 3.3 [51] while having $B(E2; 4_1^+ \rightarrow 2_1^+)/B(E2; 2_1^+ \rightarrow 0_1^+)$ ratios smaller than 2 can be characterized as soft rotors, as already suggested by Daugas *et al.* [52].

Large-scale shell-model calculations using the modified LNPS interaction [4,27], also shown in Fig. 7, accurately reproduce the $B(E2; 4_1^+ \rightarrow 2_1^+)$ values within the experimental errors. For the effective charges, we have adopted those deduced in Ref. [53]: $e_n = 0.46$ and $e_p = 1.31$. This increase in collectivity can be explained by a decrease of the subshell gap at $N = 40$, driven by the monopole proton-neutron part of the effective interaction, favoring neutron excitations into the quasi-SU(3) partners $\nu 1g_{9/2}$-$\nu 2d_{5/2}$. The occupation number for the $\nu 1g_{9/2}$ orbital increases from 1.14 for the 4_1^+ state

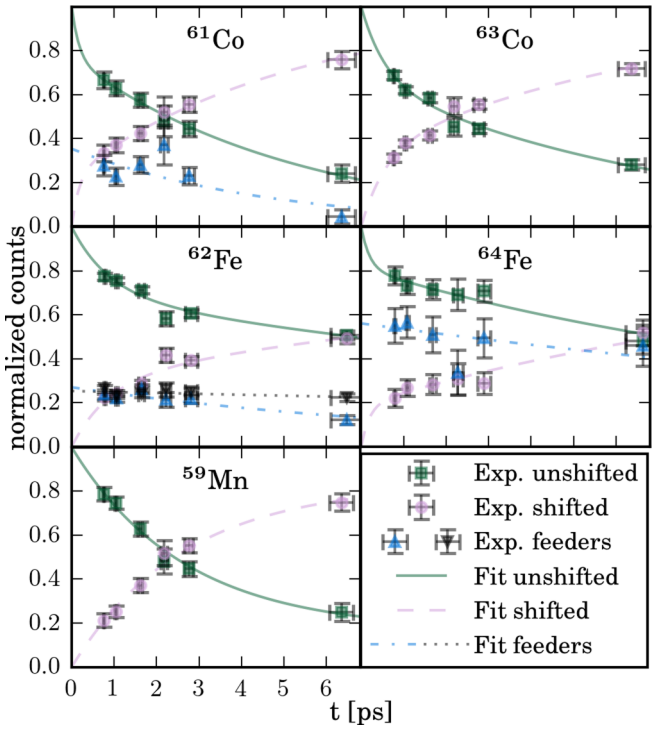

FIG. 6. The decay curves used to extract the lifetime of the $11/2^-_1$ states in ^{59}Mn and ^{61,63}Co and the 4^+_1 state in ^{62,64}Fe. Note that, for ^{62}Fe, two observed feeder states have been included in the fit. For ^{64}Fe the fit used to extract the upper limit on the lifetime is shown.

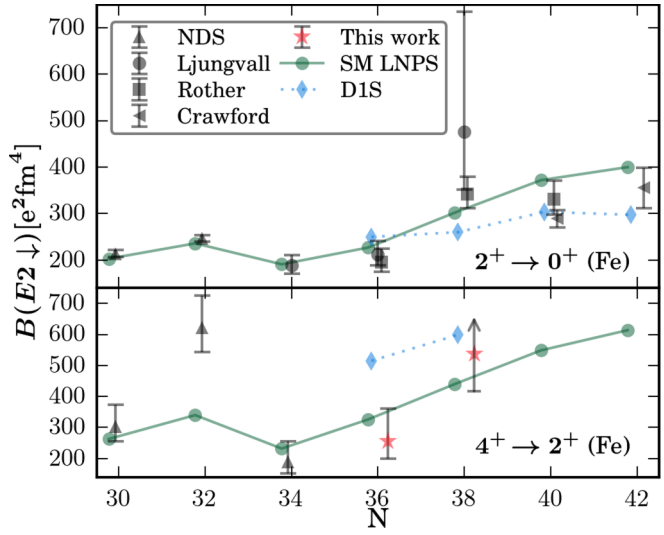

FIG. 7. $B(E2\downarrow)$ values for even iron isotopes for transitions from the first 2^+ and the first 4^+ state. The solid green lines with circles are shell-model calculations and the blue dashed lines with diamonds are D1S calculations, both a part of the present work. Previous experimental results with error bars are from Refs. [8,25,26] and Nuclear Data Sheets (NDS) [54–56], while the red stars are the new experimental results presented here.

in ^{62}Fe to 2.13 in ^{64}Fe. In relative terms the increase of occupation in the $\nu 2d_{5/2}$ orbital from $N = 36$ to $N = 38$ is even larger, going from 0.1 to 0.35 for the 4^+_1 states. On the proton side this is accompanied by an increase in the occupation of the $2p_{3/2}$ orbital, which is a quasi-SU(3) partner of the $1f_{7/2}$ orbital. The gain in energy due to the quadrupole correlations largely exceeds the energy needed to excite nucleons to the higher-lying orbitals.

We have also performed microscopic calculations based on constrained Hartree–Fock–Bogoliubov (CHFB) theory using the Gogny D1S interaction [57,58] and mapping to the five-dimensional collective Hamiltonian (5DCH). The method is described in detail in Ref. [59]. Worth noticing is that the CHFB + 5DCH calculations contain no free parameters except for those specifying the phenomenological D1S interaction, which is used across the entire nuclear chart. As can be seen in Fig. 7, these calculations give a relative increase in the $B(E2; 4^+_1 \rightarrow 2^+_1)$ values with neutron number that is very similar compared with the increase found in the shell-model calculations, but the absolute values are approximately twice as large. While the calculated $B(E2; 4^+_1 \rightarrow 2^+_1)$ value for ^{64}Fe is consistent with the experimental limit, the value for ^{62}Fe is too large. The $B(E2; 2^+_1 \rightarrow 0^+_1)$ values obtained with the 5DCH approach, on the other hand, are in good agreement with both experiment and shell-model calculations. Based on the transition strengths the results of the 5DCH calculations indicate a vibrational rather than rotational character for the neutron-rich Fe isotopes. The occupation numbers for the $\pi 1f_{7/2}$ and $\pi 2p_{3/2}$ orbitals are constant for the iron isotopes, with the latter remaining small, showing no increase of proton excitations across the $Z = 28$ shell gap, contrary to the shell-model predictions. Furthermore, at the mean-field level there are no signs of a weakening of the $N = 40$ subshell gap [35,52]. A similar result was found for neutron-rich zinc isotopes, where the 5DCH calculations also overestimated the $B(E2; 4^+_1 \rightarrow 2^+_1)$ values by a factor of two to three [60]. The 5DCH calculations provide dynamical deformed shapes for the ground state, 2^+, 4^+, and 6^+ yrast levels that are not strong enough. These discrepancies could be due to the missing of an explicit tensor term in the effective NN interaction in the Gogny D1S force. Work on implementation of such a term is currently in progress [61]. It should also be mentioned that the collective behavior assumed in the generator coordinate method (GCM) with the Gaussian overlap approximation (GOA) may not be valid close to the $Z = 28$ shell closure. The potential-energy surface obtained from the CHFB calculations shows softness in both β and γ deformation parameters, indicating no deformed minima in the iron region.

In neutron-rich cobalt isotopes a set of low-lying states has been interpreted as the $7/2^-$ proton hole weakly coupled to the 2^+ excitation in the corresponding nickel isotope; see, e.g., Refs. [16,17] and references therein. In particular it is expected that the first $11/2^-$ state belongs to this multiplet and, therefore, the $B(E2; 11/2^-_1 \rightarrow 7/2^-_1)$ values in the chain of cobalt isotopes should closely follow the $B(E2; 2^+_1 \rightarrow 0^+_1)$ values in the respective nickel isotones. In Fig. 8 the reduced transition strengths for the decay of the first 2^+ state in nickel isotopes are compared with that of the decay of the first $11/2^-$ state in the cobalt isotopes. Also shown are large-scale shell-model calculations based on the modified LNPS

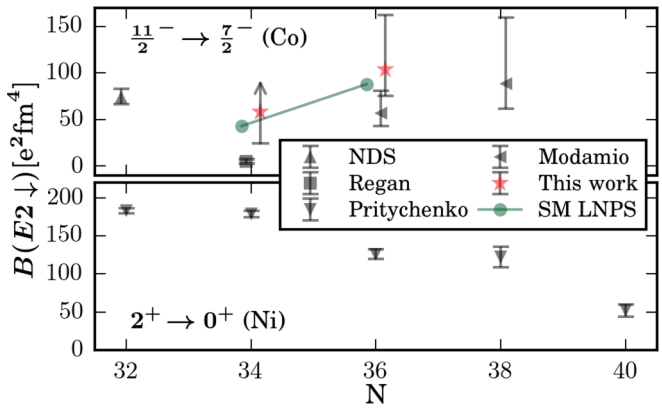

FIG. 8. $B(E2\downarrow)$ values for odd cobalt isotopes for transitions from the first $11/2^-$ to the ground state. The green solid line with circles represents shell-model calculations performed within this work. Previous experimental results with error bars are from Refs. [18,36] and the compilations [47,62] while the red stars are the new experimental results presented here. For comparison, the $B(E2\downarrow)$ values for the first 2^+ state in the even nickel isotopes are shown also.

interaction [4,27]. The new data points in this work are marked with stars. Although it was only possible to extract a lower limit for the transition probability in ^{61}Co ($N = 34$), it is clear that the result is incompatible with the older measurement from the work of Regan *et al.* who deduced 10^{+10}_{-3} ps [36]. Taking this into consideration, the hypothesis that the first $11/2^-$ state in the neutron-rich cobalt isotopes belongs to the multiplet generated by the coupling of the $7/2^-$ proton hole to the 2^+ state in the nickel isotopes is a good first-order understanding of their structure. The shell-model calculations reproduce very well the experimental data. Analyzing them in detail shows that both ^{61}Co and ^{63}Co lie outside the island of inversion below ^{68}Ni, where an increased population of quasi-SU(3) partner orbitals ($\nu 1g_{9/2}$-$\nu 2d_{5/2}$) generates quadrupole correlations. The occupation numbers for the $\nu 1g_{9/2}$ orbital remain small, around 0.1 for ^{61}Co and 0.5 for ^{63}Co for the first $11/2^-$ states. The $\nu 2d_{5/2}$ orbital is very weakly populated as well. Calculations restricted to a fp model space reproduce the excitation energies, and to a lesser extent also the transition strengths. This suggests that ^{61,63}Co can be viewed as being on the limit of the fp space, as was already concluded by Recchia *et al.* [17].

Only few transition strengths are known for the manganese isotopes, in particular for the $11/2^-_1 \rightarrow 7/2^-_1$ transition. The systematics of the $11/2^-_1$ level in the neutron-rich manganese isotopes ($A = 55$–61) shows rather constant energies with no signs of rapid changes in its structure. In ^{55}Mn the $B(E2; 11/2^-_1 \rightarrow 7/2^-_1)$ has been determined to be 167(20) e^2 fm^4 [63], to be compared with 110^{+15}_{-12} e^2 fm^4 in ^{59}Mn as measured in this work. Our calculations overestimate the $B(E2; 11/2^-_1 \rightarrow 7/2^-_1)$ value in ^{59}Mn, but remain smaller than the $B(E2; 11/2^-_1 \rightarrow 7/2^-_1)$ value in ^{55}Mn. Hence, neither the experimental nor the theoretical result show any sign of enhanced collectivity for ^{59}Mn. This is consistent with recent collinear laser spectroscopy studies of Babcock *et al.* [30], which suggest an increase of collectivity due to a weakening of the $N = 40$ subshell closure beyond $N = 36$.

TABLE I. Summary of experimental and theoretical lifetimes and $B(E2)$ values obtained in this work. Previously measured lifetimes are also given with corresponding reference.

Nuc.	State	γ energy	τ [ps]		$B(E2\downarrow)$ [e^2 fm^4]		
		[keV]	Expt.	Prev.	Expt.	SM	D1S
^{59}Mn	$11/2^-_1$	1189	2.63(40)		111^{+21}_{-15}	152	
^{62}Fe	4^+_1	1299	0.86(25)		256^{+105}_{-58}	326	515
^{64}Fe	4^+_1	1017	<1.8		>420	441	599
^{61}Co	$11/2^-_1$	1664	<2	10^{+10}_{-3} [36]	>24	43	
^{63}Co	$11/2^-_1$	1672	0.55(19)	1.0(3) [18]	104^{+58}_{-28}	88	

VI. SUMMARY

In the present work, lifetimes of excited states in moderately-neutron-rich cobalt, iron, and manganese isotopes have been measured by using the recoil distance Doppler shift method. The nuclei ^{61,63}Co, ^{62,64}Fe, and ^{59}Mn were produced in an experiment at GANIL via multinucleon transfer reactions of a ^{238}U beam on a ^{64}Ni target, identified on an event-by-event basis in the large-acceptance spectrometer VAMOS++, and γ rays were detected using the AGATA γ-ray spectrometer. It was possible to determine the lifetime of the 4^+_1 state in ^{62}Fe and give an upper limit for ^{64}Fe. For the odd-Z neighbor isotopes, lifetimes for the $11/2^-$ states in ^{59}Mn and ^{63}Co were determined, whereas for ^{61}Co again only an upper limit could be given. Theoretical calculations have been performed and compared with the experimental results, as summarized in Table I. Large-scale shell-model calculations using the modified LNPS interaction [4,27] give a very good description of the low-energy nuclear structure in the region. They show an increase in quadrupole collectivity when approaching $N = 40$. Quadrupole correlations induce the excitation of neutrons to the $\nu 1g_{9/2}$ and $\nu 2d_{5/2}$ orbitals. For the even-even iron isotopes, a rotational-like behavior emerges as $N = 40$ is approached. In the case of ^{59}Mn, the predicted transition probability for the $11/2^-_1 \rightarrow 7/2^-_1$ transition is larger than the measured one. It should be pointed out that our shell-model calculations are capable of reproducing both excitation energies and transition probabilities for nuclei both inside and outside of the island of inversion found at $N = 40$.

Beyond-mean-field CHFB + 5DCH calculations using the D1S interaction were also compared with the experimental data. Although the overall trend of increasing collectivity with increasing neutron number for the iron isotopes is clearly seen, the beyond-mean-field calculations suggest a vibrational-like structure and no clear change in structure close to $N = 38$. This might originate from the lack of an explicit tensor term in the force.

ACKNOWLEDGMENTS

We are grateful for the help from Johan Goupil and the GANIL technical staff. The authors would also like to thank M. Loriggiola, Laboratori Nazionali di Legnaro, and

G. Fremont, GANIL, for preparing the target and degrader foils. This project received funding from the European Union's Horizon 2020 research and innovation programme under grant agreement n°654002. Support from the Norwegian Research Council, project grant 213442, is acknowledged. The project has received funding from the Swedish Research Council. This work is supported by the Spanish Ministerio de Economía y Competitividad under contract FPA2014-57196-C5-4-P. One of the authors, A. Gadea, was partially supported by MINECO and Generalitat Valenciana, Spain, under the grants FPA2014-57196-C5 and PROMETEOII/2014/019, and by EU FEDER funds.

[1] O. Sorlin and M.-G. Porquet, Prog. Part. Nucl. Phys. **61**, 602 (2008).
[2] T. Otsuka, R. Fujimoto, Y. Utsuno, B. A. Brown, M. Honma, and T. Mizusaki, Phys. Rev. Lett. **87**, 082502 (2001).
[3] T. Otsuka, T. Suzuki, R. Fujimoto, H. Grawe, and Y. Akaishi, Phys. Rev. Lett. **95**, 232502 (2005).
[4] S. M. Lenzi, F. Nowacki, A. Poves, and K. Sieja, Phys. Rev. C **82**, 054301 (2010).
[5] P. C. Srivastava and V. K. B. Kota, Phys. At. Nucl. **74**, 971 (2011).
[6] J. Kotila and S. M. Lenzi, Phys. Rev. C **89**, 064304 (2014).
[7] L. Coraggio, A. Covello, A. Gargano, and N. Itaco, Phys. Rev. C **89**, 024319 (2014).
[8] J. Ljungvall, A. Görgen, A. Obertelli, W. Korten, E. Clément, G. de France, A. Bürger, J.-P. Delaroche, A. Dewald, A. Gadea *et al.*, Phys. Rev. C **81**, 061301 (2010).
[9] R. Broda, B. Fornal, W. Królas, T. Pawłat, D. Bazzacco, S. Lunardi, C. Rossi-Alvarez, R. Menegazzo, G. de Angelis, P. Bednarczyk, J. Rico, D. De Acuña, P. J. Daly, R. H. Mayer, M. Sferrazza, H. Grawe, K. H. Maier, and R. Schubart, Phys. Rev. Lett. **74**, 868 (1995).
[10] O. Sorlin, S. Leenhardt, C. Donzaud, J. Duprat, F. Azaiez, F. Nowacki, H. Grawe, Z. Dombrádi, F. Amorini, A. Astier, D. Baiborodin, M. Belleguic, C. Borcea, C. Bourgeois, D. M. Cullen, Z. Dlouhy, E. Dragulescu, M. Górska, S. Grévy, D. Guillemaud-Mueller, G. Hagemann, B. Herskind, J. Kiener, R. Lemmon, M. Lewitowicz, S. M. Lukyanov, P. Mayet, F. de Oliveira Santos, D. Pantalica, Y.-E. Penionzhkevich, F. Pougheon, A. Poves, N. Redon, M. G. Saint-Laurent, J. A. Scarpaci, G. Sletten, M. Stanoiu, O. Tarasov, and C. Theisen, Phys. Rev. Lett. **88**, 092501 (2002).
[11] C. Guénaut, G. Audi, D. Beck, K. Blaum, G. Bollen, P. Delahaye, F. Herfurth, A. Kellerbauer, H.-J. Kluge, J. Libert, D. Lunney, S. Schwarz, L. Schweikhard, and C. Yazidjian, Phys. Rev. C **75**, 044303 (2007).
[12] S. Rahaman, J. Hakala, V. V. Elomaa, T. Eronen, U. Hager, A. Jokinen, A. Kankainen, I. D. Moore, H. Penttilä, S. Rinta-Antila, J. Rissanen, A. Saastamoinen, C. Weber, and J. Äystö, Eur. Phys. J. A **34**, 5 (2007).
[13] K. Langanke, J. Terasaki, F. Nowacki, D. J. Dean, and W. Nazarewicz, Phys. Rev. C **67**, 044314 (2003).
[14] D. Pauwels, O. Ivanov, N. Bree, J. Büscher, T. E. Cocolios, J. Gentens, M. Huyse, A. Korgul, Y. Kudryavtsev, R. Raabe, M. Sawicka, I. Stefanescu, J. Van de Walle, P. Van den Bergh, P. Van Duppen, and W. B. Walters, Phys. Rev. C **78**, 041307(R) (2008).
[15] D. Pauwels, O. Ivanov, N. Bree, J. Büscher, T. E. Cocolios, M. Huyse, Y. Kudryavtsev, R. Raabe, M. Sawicka, J. Van de Walle, P. Van Duppen, A. Korgul, I. Stefanescu, A. A. Hecht, N. Hoteling, A. Wöhr, W. B. Walters, R. Broda, B. Fornal, W. Krolas, T. Pawlat, J. Wrzesinski, M. P. Carpenter, R. V. F. Janssens, T. Lauritsen, D. Seweryniak, S. Zhu, J. R. Stone, and X. Wang, Phys. Rev. C **79**, 044309 (2009).
[16] A. Dijon, E. Clément, G. de France, P. Van Isacker, J. Ljungvall, A. Görgen, A. Obertelli, W. Korten, A. Dewald, A. Gadea *et al.*, Phys. Rev. C **83**, 064321 (2011).
[17] F. Recchia, S. M. Lenzi, S. Lunardi, E. Farnea, A. Gadea, N. Mărginean, D. R. Napoli, F. Nowacki, A. Poves, J. J. Valiente-Dobón, M. Axiotis, S. Aydin, D. Bazzacco, G. Benzoni, P. G. Bizzeti, A. M. Bizzeti-Sona, A. Bracco, D. Bucurescu, E. Caurier, L. Corradi, G. de Angelis, F. Della Vedova, E. Fioretto, A. Gottardo, M. Ionescu-Bujor, A. Iordachescu, S. Leoni, R. Mărginean, P. Mason, R. Menegazzo, D. Mengoni, B. Million, G. Montagnoli, R. Orlandi, G. Pollarolo, E. Sahin, F. Scarlassara, R. P. Singh, A. M. Stefanini, S. Szilner, C. A. Ur, and O. Wieland, Phys. Rev. C **85**, 064305 (2012).
[18] V. Modamio, J. J. Valiente-Dobón, S. Lunardi, S. M. Lenzi, A. Gadea, D. Mengoni, D. Bazzacco, A. Algora, P. Bednarczyk, G. Benzoni *et al.*, Phys. Rev. C **88**, 044326 (2013).
[19] M. Hannawald, T. Kautzsch, A. Wöhr, W. B. Walters, K.-L. Kratz, V. N. Fedoseyev, V. I. Mishin, W. Böhmer, B. Pfeiffer, V. Sebastian, Y. Jading, U. Köster, J. Lettry, H. L. Ravn, and ISOLDE Collaboration, Phys. Rev. Lett. **82**, 1391 (1999).
[20] S. N. Liddick, B. Abromeit, A. Ayres, A. Bey, C. R. Bingham, B. A. Brown, L. Cartegni, H. L. Crawford, I. G. Darby, R. Grzywacz, S. Ilyushkin, M. Hjorth-Jensen, N. Larson, M. Madurga, D. Miller, S. Padgett, S. V. Paulauskas, M. M. Rajabali, K. Rykaczewski, and S. Suchyta, Phys. Rev. C **87**, 014325 (2013).
[21] G. Benzoni, A. Morales, H. Watanabe, S. Nishimura, L. Coraggio, N. Itaco, A. Gargano, F. Browne, R. Daido, P. Doornenbal, Y. Fang, G. Lorusso, Z. Patel, S. Rice, L. Sinclair, P.-A. Söderström, T. Sumikama, J. Wu, Z. Xu, R. Yokoyama, H. Baba, R. Avigo, F. B. Garrote, N. Blasi, A. Bracco, F. Camera, S. Ceruti, F. Crespi, G. de Angelis, M.-C. Delattre, Z. Dombradi, A. Gottardo, T. Isobe, I. Kuti, K. Matsui, B. Melon, D. Mengoni, T. Miyazaki, V. Modamio-Hoybjor, S. Momiyama, D. Napoli, M. Niikura, R. Orlandi, H. Sakurai, E. Sahin, D. Sohler, R. Taniuchi, J. Taprogge, Z. Vajta, J. Valiente-Dobón, O. Wieland, and M. Yalcinkaya, Phys. Lett. B **751**, 107 (2015).
[22] N. Hoteling, W. B. Walters, R. V. F. Janssens, R. Broda, M. P. Carpenter, B. Fornal, A. A. Hecht, M. Hjorth-Jensen, W. Królas, T. Lauritsen, T. Pawlat, D. Seweryniak, X. Wang, A. Wöhr, J. Wrzesiński, and S. Zhu, Phys. Rev. C **74**, 064313 (2006).
[23] S. Lunardi, S. M. Lenzi, F. Della Vedova, E. Farnea, A. Gadea, N. Marginean, D. Bazzacco, S. Beghini, P. G. Bizzeti, A. M. Bizzeti-Sona, D. Bucurescu, L. Corradi, A. N. Deacon, G. de Angelis, E. Fioretto, S. J. Freeman, M. Ionescu-Bujor, A. Iordachescu, P. Mason, D. Mengoni, G. Montagnoli, D. R. Napoli, F. Nowacki, R. Orlandi, G. Pollarolo, F. Recchia, F. Scarlassara, J. F. Smith, A. M. Stefanini, S. Szilner, C. A. Ur,

J. J. Valiente-Dobón, and B. J. Varley, Phys. Rev. C **76**, 034303 (2007).
[24] P. Adrich, A. M. Amthor, D. Bazin, M. D. Bowen, B. A. Brown, C. M. Campbell, J. M. Cook, A. Gade, D. Galaviz, T. Glasmacher, S. McDaniel, D. Miller, A. Obertelli, Y. Shimbara, K. P. Siwek, J. A. Tostevin, and D. Weisshaar, Phys. Rev. C **77**, 054306 (2008).
[25] W. Rother, A. Dewald, H. Iwasaki, S. M. Lenzi, K. Starosta, D. Bazin, T. Baugher, B. A. Brown, H. L. Crawford, C. Fransen, A. Gade, T. N. Ginter, T. Glasmacher, G. F. Grinyer, M. Hackstein, G. Ilie, J. Jolie, S. McDaniel, D. Miller, P. Petkov, T. Pissulla, A. Ratkiewicz, C. A. Ur, P. Voss, K. A. Walsh, D. Weisshaar, and K.-O. Zell, Phys. Rev. Lett. **106**, 022502 (2011).
[26] H. L. Crawford, R. M. Clark, P. Fallon, A. O. Macchiavelli, T. Baugher, D. Bazin, C. W. Beausang, J. S. Berryman, D. L. Bleuel, C. M. Campbell, M. Cromaz, G. de Angelis, A. Gade, R. O. Hughes, I. Y. Lee, S. M. Lenzi, F. Nowacki, S. Paschalis, M. Petri, A. Poves, A. Ratkiewicz, T. J. Ross, E. Sahin, D. Weisshaar, K. Wimmer, and R. Winkler, Phys. Rev. Lett. **110**, 242701 (2013).
[27] C. Santamaria, C. Louchart, A. Obertelli, V. Werner, P. Doornenbal, F. Nowacki, G. Authelet, H. Baba, D. Calvet, F. Château, A. Corsi, A. Delbart, J.-M. Gheller, A. Gillibert, T. Isobe, V. Lapoux, M. Matsushita, S. Momiyama, T. Motobayashi, M. Niikura, H. Otsu, C. Péron, A. Peyaud, E. C. Pollacco, J.-Y. Roussé, H. Sakurai, M. Sasano, Y. Shiga, S. Takeuchi, R. Taniuchi, T. Uesaka, H. Wang, K. Yoneda, F. Browne, L. X. Chung, Z. Dombradi, S. Franchoo, F. Giacoppo, A. Gottardo, K. Hadynska-Klek, Z. Korkulu, S. Koyama, Y. Kubota, J. Lee, M. Lettmann, R. Lozeva, K. Matsui, T. Miyazaki, S. Nishimura, L. Olivier, S. Ota, Z. Patel, N. Pietralla, E. Sahin, C. Shand, P.-A. Söderström, I. Stefan, D. Steppenbeck, T. Sumikama, D. Suzuki, Z. Vajta, J. Wu, and Z. Xu, Phys. Rev. Lett. **115**, 192501 (2015).
[28] J. J. Valiente-Dobón, S. M. Lenzi, S. J. Freeman, S. Lunardi, J. F. Smith, A. Gottardo, F. D. Vedova, E. Farnea, A. Gadea, D. R. Napoli *et al.*, Phys. Rev. C **78**, 024302 (2008).
[29] D. Steppenbeck, A. N. Deacon, S. J. Freeman, R. V. F. Janssens, S. Zhu, M. P. Carpenter, P. Chowdhury, M. Honma, T. Lauritsen, C. J. Lister *et al.*, Phys. Rev. C **81**, 014305 (2010).
[30] C. Babcock, H. Heylen, J. Billowes, M. Bissell, K. Blaum, P. Campbell, B. Cheal, R. G. Ruiz, C. Geppert, W. Gins, M. Kowalska, K. Kreim, S. Lenzi, I. Moore, R. Neugart, G. Neyens, W. Nörtershäuser, J. Papuga, and D. Yordanov, Phys. Lett. B **750**, 176 (2015).
[31] Z. H. Wang, J. Xiang, W. H. Long, and Z. P. Li, J. Phys. G **42**, 045108 (2015).
[32] K. Yoshida and N. Hinohara, Phys. Rev. C **83**, 061302 (2011).
[33] K. Sato, N. Hinohara, K. Yoshida, T. Nakatsukasa, M. Matsuo, and K. Matsuyanagi, Phys. Rev. C **86**, 024316 (2012).
[34] C. F. Jiao, J. C. Pei, and F. R. Xu, Phys. Rev. C **90**, 054314 (2014).
[35] L. Gaudefroy, A. Obertelli, S. Péru, N. Pillet, S. Hilaire, J. P. Delaroche, M. Girod, and J. Libert, Phys. Rev. C **80**, 064313 (2009).
[36] P. H. Regan, J. W. Arrison, U. J. Hüttmeier, and D. P. Balamuth, Phys. Rev. C **54**, 1084 (1996).
[37] J. Van de Walle, V. Bildstein, N. Bree, J. Cederkäll, P. Delahaye, J. Diriken, A. Ekström, V. N. Fedosseev, R. Gernhäuser, A. Gustafsson, A. Herlert, M. Huyse, O. Ivanov, T. Kröll, R. Krücken, B. Marsh, N. Partronis, P. Van Duppen, D. Voulot, N. Warr, F. Wenander, K. Wimmer, and S. M. Lenzi, Eur. Phys. J. A **42**, 401 (2009).
[38] T. Baugher, A. Gade, R. V. F. Janssens, S. M. Lenzi, D. Bazin, M. P. Carpenter, C. J. Chiara, A. N. Deacon, S. J. Freeman, G. F. Grinyer, C. R. Hoffman, B. P. Kay, F. G. Kondev, T. Lauritsen, E. M. Lunderberg, S. McDaniel, K. C. Meierbachtol, A. Ratkiewicz, S. R. Stroberg, K. A. Walsh, D. Weisshaar, and S. Zhu, Phys. Rev. C **93**, 014313 (2016).
[39] A. Dewald, O. Möller, and P. Petkov, Prog. Part. Nucl. Phys. **67**, 786 (2012).
[40] S. Pullanhiotan, M. Rejmund, A. Navin, W. Mittig, and S. Bhattacharyya, Nucl. Instrum. Methods Phys. Res., Sect. A **593**, 343 (2008).
[41] M. Rejmund, B. Lecornu, A. Navin, C. Schmitt, S. Damoy, O. Delaune, J. Enguerrand, G. Fremont, P. Gangnant, L. Gaudefroy, B. Jacquot, J. Pancin, S. Pullanhiotan, and C. Spitaels, Nucl. Instrum. Methods Phys. Res., Sect. A **646**, 184 (2011).
[42] M. Vandebrouck, A. Lemasson, M. Rejmund, G. Fremont, J. Pancin, A. Navin, C. Michelagnoli, J. Goupil, C. Spitaels, and B. Jacquot, Nucl. Instrum. Methods Phys. Res., Sect. A **812**, 112 (2016).
[43] S. Akkoyun, A. Algora, B. Alikhani, F. Ameil, G. de Angelis, L. Arnold, A. Astier, A. Ataç, Y. Aubert, C. Aufranc *et al.*, Nucl. Instrum. Methods Phys. Res., Sect. A **668**, 26 (2012).
[44] E. Clément (unpublished).
[45] J. Ljungvall, G. Georgiev, S. Cabaret, N. Karkour, D. Linget, G. Sedes, R. Chevrier, I. Matea, M. Niikura, M.-D. Salsac, and B. Sulignano, Nucl. Instrum. Methods Phys. Res., Sect. A **679**, 61 (2012).
[46] E. Farnea, F. Recchia, D. Bazzacco, T. Kröll, Z. Podolyák, B. Quintana, and A. Gadea, Nucl. Instrum. Methods Phys. Res., Sect. A **621**, 331 (2010).
[47] B. Pritychenko, J. Choquette, M. Horoi, B. Karamy, and B. Singh, At. Data Nucl. Data Tables **98**, 798 (2012).
[48] O. Kenn, K.-H. Speidel, R. Ernst, J. Gerber, N. Benczer-Koller, G. Kumbartzki, P. Maier-Komor, and F. Nowacki, Phys. Rev. C **63**, 021302 (2000).
[49] J. M. Allmond, B. A. Brown, A. E. Stuchbery, A. Galindo-Uribarri, E. Padilla-Rodal, D. C. Radford, J. C. Batchelder, M. E. Howard, J. F. Liang, B. Manning, R. L. Varner, and C.-H. Yu, Phys. Rev. C **90**, 034309 (2014).
[50] E. K. Warburton, J. W. Olness, A. M. Nathan, J. J. Kolata, and J. B. McGrory, Phys. Rev. C **16**, 1027 (1977).
[51] L. Grodzins, Phys. Lett. **2**, 88 (1962).
[52] J. M. Daugas, I. Matea, J.-P. Delaroche, M. Pfützner, M. Sawicka, F. Becker, G. Bélier, C. R. Bingham, R. Borcea, E. Bouchez, A. Buta, E. Dragulescu, G. Georgiev, J. Giovinazzo, M. Girod, H. Grawe, R. Grzywacz, F. Hammache, F. Ibrahim, M. Lewitowicz, J. Libert, P. Mayet, V. Méot, F. Negoita, F. de Oliveira Santos, O. Perru, O. Roig, K. Rykaczewski, M. G. Saint-Laurent, J. E. Sauvestre, O. Sorlin, M. Stanoiu, I. Stefan, C. Stodel, C. Theisen, D. Verney, and J. Żylicz, Phys. Rev. C **83**, 054312 (2011).
[53] M. Dufour and A. P. Zuker, Phys. Rev. C **54**, 1641 (1996).
[54] H. Junde, H. Su, and Y. Dong, Nucl. Data Sheets **112**, 1513 (2011).
[55] C. D. Nesaraja, S. D. Geraedts, and B. Singh, Nucl. Data Sheets **111**, 897 (2010).
[56] E. Browne and J. Tuli, Nucl. Data Sheets **114**, 1849 (2013).
[57] J. Dechargé and D. Gogny, Phys. Rev. C **21**, 1568 (1980).

[58] J. Berger, M. Girod, and D. Gogny, Comput. Phys. Commun. **63**, 365 (1991).
[59] J. P. Delaroche, M. Girod, J. Libert, H. Goutte, S. Hilaire, S. Péru, N. Pillet, and G. F. Bertsch, Phys. Rev. C **81**, 014303 (2010).
[60] C. Louchart, A. Obertelli, A. Görgen, W. Korten, D. Bazzacco, B. Birkenbach, B. Bruyneel, E. Clément, P. J. Coleman-Smith, L. Corradi, D. Curien, G. de Angelis, G. de France, J.-P. Delaroche, A. Dewald, F. Didierjean, M. Doncel, G. Duchêne, J. Eberth, M. N. Erduran, E. Farnea, C. Finck, E. Fioretto, C. Fransen, A. Gadea, M. Girod, A. Gottardo, J. Grebosz, T. Habermann, M. Hackstein, T. Huyuk, J. Jolie, D. Judson, A. Jungclaus, N. Karkour, S. Klupp, R. Krücken, A. Kusoglu, S. M. Lenzi, J. Libert, J. Ljungvall, S. Lunardi, G. Maron, R. Menegazzo, D. Mengoni, C. Michelagnoli, B. Million, P. Molini, O. Möller, G. Montagnoli, D. Montanari, D. R. Napoli, R. Orlandi, G. Pollarolo, A. Prieto, A. Pullia, B. Quintana, F. Recchia, P. Reiter, D. Rosso, W. Rother, E. Sahin, M.-D. Salsac, F. Scarlassara, M. Schlarb, S. Siem, P. P. Singh, P.-A. Söderström, A. M. Stefanini, O. Stézowski, B. Sulignano, S. Szilner, C. Theisen, C. A. Ur, J. J. Valiente-Dobón, and M. Zielinska, Phys. Rev. C **87**, 054302 (2013).
[61] R. N. Bernard and M. Anguiano, Nucl. Phys. A **953**, 32 (2016).
[62] C. M. Baglin, Nucl. Data Sheets **95**, 215 (2002).
[63] A. M. Nathan, J. W. Olness, E. K. Warburton, and J. B. McGrory, Phys. Rev. C **16**, 192 (1977).